Topological solitons in a Su-Schrieffer-Heeger chain with periodic hopping modulation, domain wall, and disorder

Surajit Mandal and Satyaki Kar
Department of Physics, AKPC Mahavidyalaya, Bengai, West Bengal-712611, India

(Received 8 February 2024; accepted 22 April 2024; published 8 May 2024)

A chiral symmetric Su-Schrieffer-Heeger (SSH) chain features topological end states in one of its dimerized configurations. Those midgap zero-energy states show interesting modifications upon a periodic tuning of the hopping modulations. In addition, more and more in-gap end modes appear at nonzero energies for further partitioning of the Brillouin zone (BZ) due to increased hopping periodicity. These topological phases are identified with a detailed analysis of the topological invariants, namely, winding number and Zak phases. The spectra and topology of these systems with periodically modulated hopping are also studied in the presence of a single static domain wall, separating two topologically inequivalent dimerized structures. The domain wall causes additional in-gap modes in the spectrum as well as zero-energy domain-wall solitonic states for specific hopping periodicities. We also study the effect of disorder, particularly the chirality breaking on-site ones, on the edge and domain-wall states. Other than the SSH type, we also consider random, Rice-Mele, or AI-type disorder to do a comparative analysis of the evolution of chirality and zero-energy states as the strength of disorder and hopping periodicity is varied. Our findings can add important feedback in utilizing topological phases in various fields including quantum computations, while the results can be easily verified in a cold atom setup within optical lattices.

DOI: 10.1103/PhysRevB.109.195124

I. INTRODUCTION

Topology in condensed matter [1–7] is a very hot topic these days due to the renewed understanding and subsequent discoveries both in theoretical [8–12] and experimental [6,13] fronts identifying the robustness of the topological protections and its possible implementation in various fields, including quantum computations [14–16].

Today we often talk of graphene, whose discovery [17] using the Scotch tape method in 2004 turned out to be a milestone in the journey of topological condensed matter systems for its Dirac-like excitations at low energies, high mobilities, and topological stability [18]. From there, physicists moved on to topological system synthesis and analysis via the Haldane model [19], Kane-Mele model [20], topological insulators [21], and then Weyl, Dirac semimetals [22], and so forth.

Graphene has a staggered single bond-double bond structure (considering single resonance structure [23]) in a hexagonal lattice. But before it became popular, scientists were intrigued by the 1D conducting polymers involving the same staggered bonding structures. That is when the $(CH)_n$ polyacetylene chain [24] became important to the science community for its topological behavior, solitonic excitations, and domain-wall (DW) structures [25–27].

A long chain of polyacetylene has a pair of degenerate ground states for two different sets of dimerization [25]. For a finite chain, these two staggered arrangements are topologically distinct, for the end site sees either a strong or a weak bond. In the topological regime, end modes appear as zero energy states (ZESs) that peak at the boundaries and die out exponentially away from there. One can call these end solitons. In a half-filled system, their spectral weights are equally shared between unoccupied conduction and occupied valence bands. With electrons added to or removed from the half-filled system, the end modes occupy with fractionalized charges $\mp e/2$. Strictly speaking, they are bonding and antibonding small gap states and of mixed chirality. But linear combinations of them can be considered to obtain a pair of chiral ZESs that are located in single ends of the chain [28].

A Su-Schrieffer-Heeger (SSH) model that can correspond to a polyacetylene chain is a 1D tight-binding model with staggered hopping modulation [25] and can demonstrate charge fractionalizations [29,30], the existence of zero energy end states, and topological solitonic excitations [25,27]. Neutral solitons with moving domain walls having $S = \pm\frac{1}{2}$ are obtained, as the excitations though charged solitons can also found for a doped $(CH)_n$ system [26]. The SSH chain has chiral symmetry and the chain features unit cells comprising two adjacent sites. The staggered nature of the hopping brings in this two-sublattice structure in the chain and, accordingly, the chiral symmetry, here, is also familiar as sublattice symmetry. It makes the Bloch Hamiltonian off-diagonal, which gives the simplest route to derive the topological winding number, as we also have elaborated on in this paper.

In this respect, it would not be ludicrous to add a discussion on exotic Majorana fermions, that are their own antiparticles which appear as quasiparicle excitations, called Majorana bound states (MBSs) in some condensed matter systems with defects [1–3]. Our system of concern—the SSH model can be broken down to two independent Majorana hopping chains. Similarly, in a spinless Kitaev chain with p-wave pairing [31],

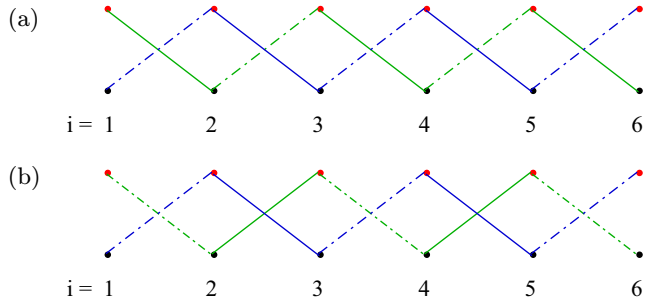

FIG. 1. Both the Kitaev chain (a) and SSH chain (b) can be broken down to two independent Majorana hopping models. When the weaker bond vanishes, end sites become disconnected from the rest of the chain. While the Kitaev chain features two MBSs localized at two ends, the SSH chain features two MBSs at each end which turn them into electronic ZESs.

a pair of independent Majorana hopping chains appear and single Majorana zero modes (MZMs) survive there at the ends. The unconventional superconducting pairing can nullify the effect of quantum zero point motion to pin the Majorana states at the zero energy. Due to their non-Abelian exchange statistics, they lead to decoherence-free quantum information processing [14]. However, for the SSH model, the pair of Majorana modes localized at each end turn them into electronic modes and we do not get any Majorana physics in this system [32], but with interaction added, Majorana modes can be incorporated in such systems.

The chiral symmetric SSH chain, with the Hamiltonian shown in Eq. (1), features a topological phase for weak bonds at the boundaries, and midgap zero energy states (ZES) with fractional charge are obtained. Figure 1 demonstrates that while in a Kitaev chain, end states are found to be Majorana modes, in the SSH model the pair of Majorana modes at each end produces electronic ZESs at two boundaries. It gets interesting when the ZES gets redistributed or modified due to a periodic variation of the hopping modulation that goes beyond simple staggered hopping of the SSH chain. A similar study has been initiated by one of the authors in Ref. [12]. In this paper, we extend the calculations incorporating detailed analysis of the winding numbers to identify the topological (nontopological) end modes of this periodically hopping modulated system. In addition, here we also consider the effect of domain wall (DW) and disorders. A static DW at the center of a SSH chain break it into two topologically inequivalent regime on its two sides and results in solitonic states in the system. The consequence of having domain walls in the SSH chain [33] and other related models [26,34–36] have been probed to some extent in the literature. Here we find that the presence of periodic modulation of hopping amplitude causes additional in-gap modes to appear. In addition, one of the end modes vanishes with new zero energy solitonic states appearing at the DW position for specific periodicities of hopping modulations. Furthermore, the addition of on-site disorder in our model leads to immediate disappearance of the chiral symmetry. We also consider random [37], Rice-Mele (RM), and AI-type of disorder [38] for comparison, which reveals that the disappearance of the ZES with disorder strength is common in all of them, though a DW state approaches zero energy for strong disorder of the AI type.

The paper is organized as follows. In Sec. II, we provide the formulation of our SSH(-like) model with periodic hopping modulation, also including a detailed analysis of symmetry and topological invariant calculations, as well as the features of spectra and end states. Next, in Sec. III, we additionally introduce a single static domain wall at the center of a finite chain and study its response on the ZES and energy spectra. Section IV describes the effect of on-site and hopping disorder in the periodically modulated chain with a domain wall which affects the chirality of the system. Finally, we summarize our results in Sec. V and discuss possible future directions of work.

II. FORMULATION

The Su-Schrieffer-Heeger (SSH) model [25], proposed in the context of polyacetylene is given by a one-dimensional tight-binding Hamiltonian with staggered nearest-neighbor (NN) hopping [thus, it shows a chiral (sublattice) symmetry]:

$$H_{\rm SSH} = \sum_{i}^{L-1}(t+\delta_i)c_i^\dagger c_{i+1} + \text{H.c.} \tag{1}$$

Here $c_i^\dagger$, c_i denotes electron creation and annihilation operator, respectively, and the periodic modulation in hopping strength (t) is obtained by $\delta_i = \Delta\cos[(i-1)\theta]$ in which $i = 1, 2, 3, \ldots, N$. In general, for $\theta = 2\pi/n$, we get $\delta_{i+1} = \Delta\cos(\frac{2\pi i}{n})$ and the chain from an n sublattice structure. Moreover, the system is represented by a $n \times n$ Hamiltonian matrix with n number of eigenmodes. The transformation $c_i \to (-1)^i c_i^\dagger$ gives $H_{\rm SSH} \to H_{\rm SSH}$, implying the sublattice or chiral symmetry [39]. For a model considering periodic boundary conditions (PBCs), chiral symmetry also needs the total number of sites to be even.

With the introduction of Majorana operators as

$$\gamma_{i,A} = \frac{1}{\sqrt{2}}(c_i^\dagger + c_i), \quad \gamma_{i,B} = \frac{i}{\sqrt{2}}(c_i^\dagger - c_i), \tag{2}$$

the Majorana representation of Eq. (1) becomes

$$H_{\rm SSH} = \sum_{i}^{L-1} i(t+\delta_i)[\gamma_{i,A}\gamma_{i+1,B} + \gamma_{i+1,A}\gamma_{i,B}]. \tag{3}$$

The case of $\theta = \pi$ corroborates the original SSH chain, which has been studied thoroughly. Here we depict the cases of a few other θ values, that are commensurate to the finite chain.

A. For $\theta = \frac{\pi}{2}$

Let us begin with a (finite) SSH(-like) chain with an open boundary condition (OBC) for $\theta = \frac{\pi}{2}$:

$$H = \sum_{i}^{L-1}(t+\Delta)c_{i,A}^\dagger c_{i,B} + t c_{i,B}^\dagger c_{i,C} + (t-\Delta)c_{i,C}^\dagger c_{i,D} + t c_{i,D}^\dagger c_{i+1,A} + \text{H.c.}, \tag{4}$$

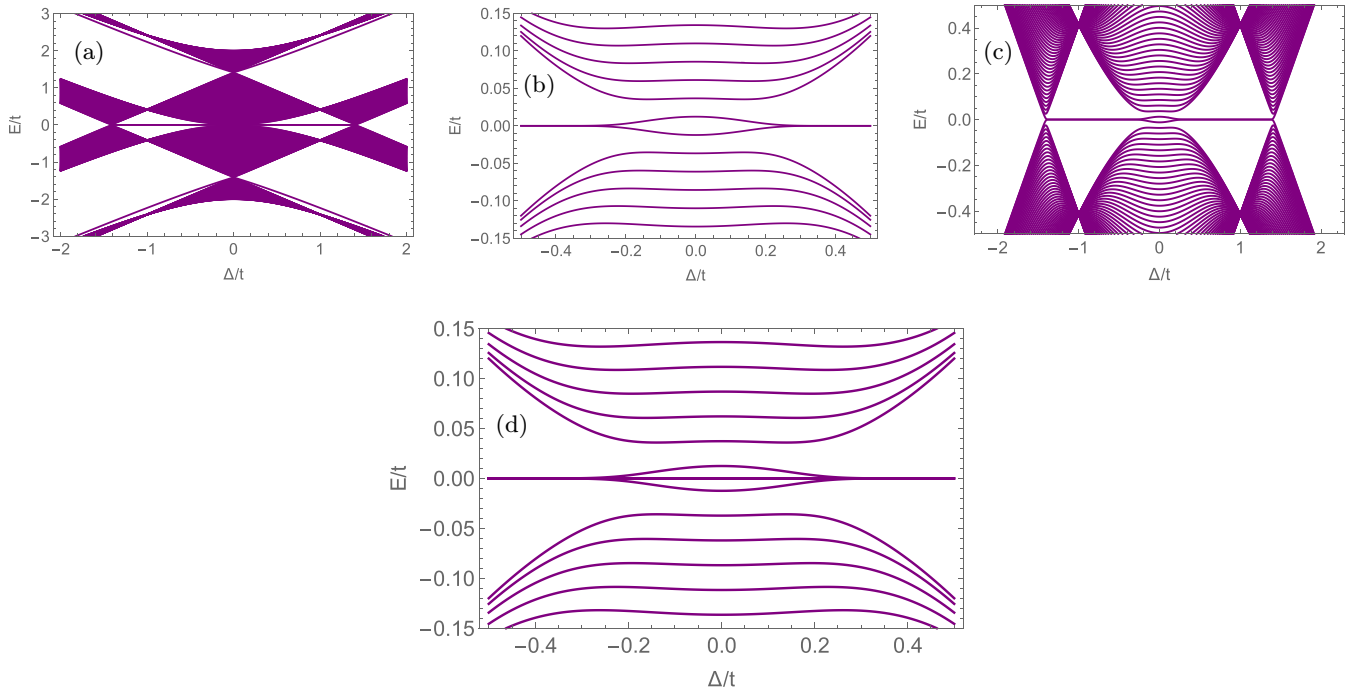

FIG. 2. (a) Spectra of a SSH(-like) chain with $L = 256$ considering OBC as a function of Δ/t for $\theta = \frac{\pi}{2}$. (b), (c) Corresponding low-energy states for $L = 256$ with smaller and larger Δ/t, respectively, while (d) represents low-energy spectra for an odd number of lattice sites with $L = 255$.

where i denotes the unit cell. For PBCs, we can consider the Fourier transform for the above Hamiltonian as

$$c_{i,\alpha} = \frac{2}{\sqrt{L}} \sum_{k\epsilon \mathrm{BZ}} e^{jki}\beta, \tag{5}$$

where $\alpha = \{A, B, C, D\}$ and $\beta = \{a_k, b_k, c_k, d_k\}$ refer to the sublattice index and the corresponding Fourier modes, respectively. Thus the Hamiltonian [Eq. (4)] in terms of the spinor field $\psi_k = (a_k, b_k, c_k, d_k)^T$ takes the form of

$$H = \sum_{k\epsilon \mathrm{BZ}} \psi_k^\dagger H_k \psi_k, \tag{6}$$

where the Bloch Hamiltonian

$$H_k = \begin{pmatrix} 0 & (t+\Delta) & 0 & te^{-4ik} \\ (t+\Delta) & 0 & t & 0 \\ 0 & t & 0 & (t-\Delta) \\ te^{4ik} & 0 & (t-\Delta) & 0 \end{pmatrix}. \tag{7}$$

The energy eigenvalues of the above matrix can be calculated as

$$\epsilon(k) = \pm\sqrt{2t^2 + \Delta^2 \pm t\sqrt{2t^2 + 6\Delta^2 + 2(t^2 - \Delta^2)\cos 4k}}. \tag{8}$$

It essentially gives four bands in the energy spectrum. Note that the energy gap closes for $\Delta = 0$ at $k = 0$ as well as for $(\Delta/t)^2 = 2$ at $k = \pm\pi/4$. Of these, the first case is a result of using the periodic boundary implied in our Fourier construction but the system gaps out there in a finite chain. However, the second case indicates a gapless point even for the finite chain and corresponds to the gap-closing topological phase transition point. The bands cross linearly there (see Fig. 3), making the low-energy modes behave as Dirac fermions [40].

The numerical energy spectra for SSH(-like) chain under OBCs for $\theta = \pi/2$ is shown in Fig. 2. The figure indicates that the energy spectra is symmetric (up-down), i.e., for every eigenstate with energy E, its chiral symmetric partner having energy $-E$ necessarily exists. Here, we get a four-sublattice configuration yielding two in-gap nonzero energy states and two ZESs. Zero-energy modes with $L = 256$ will no longer subsist for $-0.3 \lesssim \Delta/t \lesssim 0.3$ and for $\Delta/t \gtrsim 1.4$ or $\Delta/t \gtrsim -1.4$ [see, e.g., Figs. 2(b) and 2(c)].

For an odd number of lattice sites, one gets an odd number of zero-energy states. We examined that in a chain with an odd number of sites, there are L modulo 4 number of extra ZESs that are localized exactly at Mod$(L, 4)$ end sites. For example, for $L = 255$, with the spectra as shown in Fig. 2(d), there are five (for $|\Delta/t| \gtrsim 0.25$) or three (for $|\Delta/t| \lesssim 0.25$) zero energy modes (i.e., three extra ZESs) with the extra modes being localized at sites No. 253–255 (it could have been at sites No. 1–3 on the other side of the chain, had the Hamiltonian matrix taken the three extra bonds on that side).

1. Symmetry and winding number

Now we discuss a bit more on the symmetry of the SSH(-like) chain for $\theta = \frac{\pi}{2}$. By employing the chiral symmetric operator $\hat{S} = \Gamma_4 = I_2 \otimes \sigma_z$ with I_2 as the 2×2 identity matrix and σ indicating the Pauli matrices, one can check that $\{\Gamma_4, H_k\} = 0$. Hence, this Hamiltonian has a chiral symmetry (of course, for a chain with even number of sites). Apart from this, this Hamiltonian also respects the time-reversal symmetry (T) as well as particle-hole symmetry (C) and falls

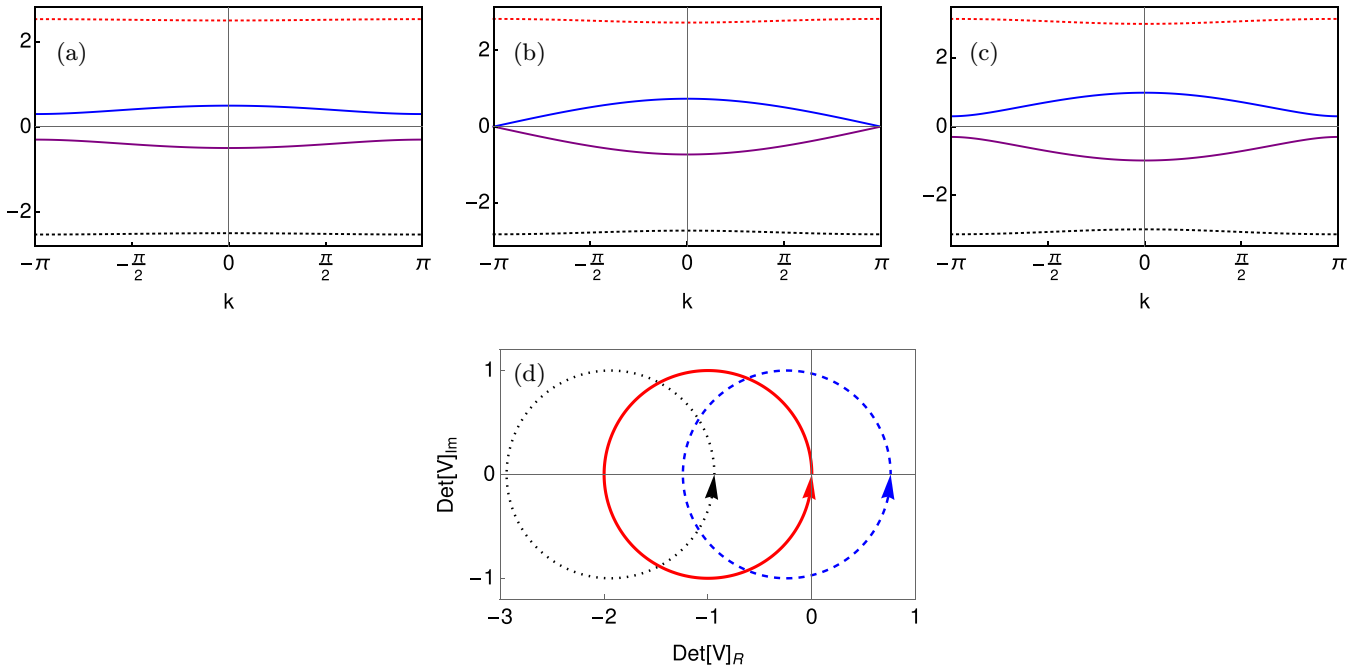

FIG. 3. The dispersion plot corresponding to $\theta = \frac{\pi}{2}$ and $\Delta/t =$ (a) $\sqrt{2} - 0.3$, (b) $\sqrt{2}$, and (c) $\sqrt{2} + 0.3$, respectively. The bottom panel shows the winding of Det(V) as k is varied through the reduced BZ, for these three cases in terms of dashed, solid, and dotted circles, respectively.

in the BDI class universality in a tenfold way classification (see Table I). Here T (C) commutes (anticommutes) with the Hamiltonian H_k which, in this spinless case, is given by $\hat{T} = I_2 \otimes I_2\mathcal{K}$ ($\hat{C} = I_2 \otimes \sigma_z\mathcal{K}$), $\mathcal{K}$ denoting the complex-conjugation). The relation $\hat{S} = \hat{T}\hat{C}$ is thus satisfied [41]. Due to the chiral symmetry of Hamiltonian, the Bloch Hamiltonian [Eq. (7)] is expected to be off-diagonal. We should add here that the presence of chiral symmetry does not necessarily ensure T and C symmetry, as there is a symmetry class called AIII that respects chiral symmetry alone. In fact, if we consider the hopping amplitudes to be complex, instead of real, then time-reversal symmetry no longer persists and $H_{\rm SSH}$ moves on to the AIII universality class [44]. The AIII class, in one dimension (1D), is always topologically nontrivial [42], unlike the usual SSH chain (with $\theta = \pi$), and its topology is described by a topological winding number.

TABLE I. Periodic table of topological invariants. Here, T, C, and S denote time-reversal symmetry, particle-hole symmetry, and and chiral symmetry operator, respectively. The value of the corresponding single-particle operator indicates the presence of symmetry. The different dimensions d can host only trivial phases, indicated by $-$, a theoretically infinite number of phases labeled by an integer $\mathbf{Z}$ or two phases, labeled by $\mathbf{Z}_2$. This table is based on Altland's and Zirnbauer's ten symmetry classes [42,43].

Class	T	C	S	$d=1$	$d=2$	$d=3$
A	0	0	0	–	$\mathbf{Z}$	–
AI	+1	0	0	–	–	–
AII	−1	0	0	–	$\mathbf{Z}_2$	$\mathbf{Z}_2$
D	0	+1	0	$\mathbf{Z}_2$	$\mathbf{Z}$	–
C	0	−1	0	–	$\mathbf{Z}$	–
AIII	0	0	1	$\mathbf{Z}$	–	$\mathbf{Z}$
BDI	+1	+1	1	$\mathbf{Z}$	–	–
CI	+1	−1	1	–	–	$\mathbf{Z}$
DIII	−1	+1	1	$\mathbf{Z}_2$	$\mathbf{Z}_2$	$\mathbf{Z}$
CII	−1	−1	1	$\mathbf{Z}$		$\mathbf{Z}_2$

There are two important corollaries of this chiral symmetry for the eigenstates and energies of the Hamiltonian. First, the energy spectrum of the SSH(-like) chain is always symmetric (up-down symmetry) in nature. For each eigenstate ψ_k having energy E, there is always another eigenstate (its chiral partner, $\Gamma_4\psi_k = \psi_k'$) with energy $-E$. Second, states with zero energy only occupy a single sublattice. When the total number of particles is odd, chiral symmetry infers that there will be an odd number of end modes having zero energy. Moreover, the energy of the in-gap end states can also be non-zero, and this symmetry implies that such states having nonzero energy should be even in number and symmetrically positioned about $E = 0$.

The one-dimensional chiral models are identified by a $\mathbf{Z}$ topological index/invariant - winding number $\mathcal{W}$ which is an integer (may be positive or negative) while in two dimensions the equivalent index is Chern number [45]. The winding number is a completely mathematical property defined for any closed and smooth curve and is defined as the number of rotations (or windings) of the winding vector (defined below) about the origin [46] as one sweeps through the first Brillouin zone (BZ). The method of calculating the winding number is not only restricted to two-band models. It is much more general and can further be defined for any multiband Hamiltonian that obeys chiral symmetry [47]. It is not always easy to determine the eigenvectors from Eq. (7) in its analytic

form. But for chiral symmetric systems, the definition of $\mathcal{W}$ can also be pertinent with the block off-diagonalized form of the Hamiltonian in the sublattice basis [48,49].

Applying the unitary transformation, the Hamiltonian H_k in Eq. (7) can be converted into block off-diagonal form

$$H_k = UH_kU^{-1} = \begin{pmatrix} 0 & V \\ V^\dagger & 0 \end{pmatrix}, \tag{9}$$

where $V(k)(V^\dagger(k))$ is 2×2 square matrices defined on the upper (lower) off-diagonal block of H_k, read

$$V(k) = \begin{pmatrix} (t+\Delta) & te^{-4ik} \\ t & (t-\Delta) \end{pmatrix} \tag{10}$$

and U is the unitary matrix obtained by employing the chiral basis as

$$U = \begin{pmatrix} 1 & 0 & 0 & 0 \\ 0 & 0 & 1 & 0 \\ 0 & 1 & 0 & 0 \\ 0 & 0 & 0 & 1 \end{pmatrix}. \tag{11}$$

Now, the calculation of the winding number can be given by [45,47]

$$\mathcal{W} = -\frac{i}{2\pi}\int_{\mathrm{BZ}} \partial_k i\phi(k)dk, \tag{12}$$

with integration on the reduced BZ, $k \in [-\pi/4, \pi/4]$ [50]. Here ϕ_k is the phase of the complex number $\mathbf{Det[V(k)]} = (t^2-\Delta^2) - t^2e^{-4ik} = R(k)e^{i\phi(k)}$. For a two-band model (see, e.g., Refs. [46,51]), one does not need to consider the determinant as $V(k)$ is just a number. However, for systems with four bands or more, this formula aims to give the topological index without further diagonalizing the Hamiltonian Eq. (7) [52]. One can substitute $\ln \mathbf{Det}[V(k)]$ in place of $i\phi_k$ in Eq. (12) [45]. Now, the winding number Eq. (12), considering the determinant, takes the form of [42,48,49,53,54]

$$\mathcal{W} = \int_{\mathrm{BZ}} \frac{dk}{2\pi i}\partial_k[\ln \mathbf{Det}[V(k)]] \tag{13}$$

and the estimate comes out to be

$$\mathcal{W} = \begin{cases} 1, & 0 < \Delta^2/t^2 < 2 \\ 0, & \Delta^2/t^2 > 2 \\ \text{undefined}, & \Delta/t = 0. \end{cases} \tag{14}$$

The complex variable $\mathbf{Det[V(k)]}$ is called the winding vector (it has a magnitude and phase angle in the complex plane, as already mentioned) as its number of winding about the origin as k varies in $[-\pi/4, \pi/4]$ [50,55] determines the winding number.

Equation (14) implies that one can get $\mathcal{W} = 1$ for small $\Delta/t \neq 0$, indicating the nontrivial topological phases (NTPs) there. But $\Delta/t = 0$ indicates an undefined $\mathcal{W}$ and hence no gap closing Lifshitz quantum phase transition (QPT) point. On the other hand, $\mathcal{W}$ remains unity until $0 < |\Delta/t| < \sqrt{2}$ and vanishes for $|\Delta/t| > \sqrt{2}$. Thus, QPT occurs at $\Delta = \pm\sqrt{2}t$ in this case. We should add here that interchanging the Majorana operators $\gamma_{i,A}$, $\gamma_{i,B}$ in Hamiltonian Eq. (3) has no significant effect (other than an overall sign change) since our considered model does not include the next-nearest-neighbor hopping amplitudes and chemical potentials. Following the above procedure, we attain

$$V'(k) = \begin{pmatrix} (t+\Delta) & t \\ te^{4ik} & (t-\Delta) \end{pmatrix}, \tag{15}$$

causing merely a sign change in the winding number: $\mathcal{W} \to -\mathcal{W}$.

It is worth mentioning that the sign changes in winding number can occur by relabelling sublattices $\{A, B, C, D\} \Leftrightarrow \{D, C, B, A\}$ (or interchanging the Majorana operators). This can also be visualized as a 'choice' of chiral symmetry operators. In the former case, it is $\hat{S} = \Gamma_4$ acting in the sublattice basis while in the latter it is $\hat{S} = -\Gamma_4$. Moreover, the sign of the winding number is related to the winding direction of winding vector **Det[V(k)]**, which in turn leads to the type of (unpaired) Majorana fermions residing at the boundary. This change of signs makes no difference when one considers a single chain, however, for multiple chains coupled to each other, such liberty no more persists as the relative sign of the individual chains becomes a relevant quantity of the system topology and the Hamiltonian no more remains block off-diagonal. Detailed illustrations of the same can be found in Ref. [45].

To change the winding number from one value to another, we are required to either close the energy gap or disturb the chiral symmetry of the system, which is the pivotal symmetry of the Hamiltonian. Moreover, breaking or preserving the chiral symmetry after the implication of on-site and hopping disorder, respectively, are discussed in Sec. IV.

The dispersion relation calculated from the bulk Hamiltonian Eq. (7) is presented in the top panel of Fig. 3. Notice that the plot indicates asymmetry of the dispersion as Δ is varied about its critical value given by $(\Delta/t)^2 = 2$—the topological phase transition points.

In the spirit of Eq. (12), one obtains

$$\mathcal{W} = \frac{1}{2\pi}[\phi(\pi/4) - \phi(-\pi/4)] = \frac{1}{2\pi}\Delta\phi. \tag{16}$$

So if **Det[V(k)]** takes m revolutions with $\Delta\phi = 2\pi m$, Eq. (16) leads to $\mathcal{W} = m$. The eigenstates are parameterized by $\phi = \tan^{-1}(\frac{\mathrm{Im[Det}(V)]}{\mathrm{Real[Det}(V)]})$. Therefore, the direction of the winding vector **Det[V(k)]** in the complex space represents an eigenstate and the magnitude of the same estimates its eigenvalue. The trajectory of **Det[V(k)]** parameterizes the evolution of the state as k is varied from $-\pi/4 \to \pi/4$. The trajectories for the asymmetric dispersion about the critical value (mentioned above) may or may not encircle the origin, indicating nontrivial or trivial topological classes, respectively.

The demonstration of the topological winding number for the 1D SSH chain (two sub-lattices) can be found in Ref. [46]. In this context, the parametric plot of the winding number in the complex plane is depicted in Fig. 3. The arrowhead stipulates the direction of movement of **Det[V(k)]** as k is varied from $-\pi/4 \to \pi/4$. The sense of rotation is in the counterclockwise direction for each of the closed contours. The contour for $\Delta/t = \sqrt{2} - 0.3$ encloses the origin making $\mathcal{W} = 1$, indicating the NTP while that for $\Delta/t = \sqrt{2} + 0.3$ does not enclose the origin and indicates a trivial topological phase (TTP) with $\mathcal{W} = 0$. The contour for $\Delta/t = \sqrt{2}$ touches

the origin and indicates the gap-closing phase-transition point [56]. This justifies our theoretical findings very well.

In Appendix A, we calculate the winding number in terms of poles and zeros, and the Berry phase for this model is studied in Appendix B [see Eq. (B1)]. Notice that the 1D polarization is the Berry phase of the occupied Bloch states. Electrostatics shows us that polarization is related to bound charges and, in the SSH chain, the Berry phase thus estimates the charges of the end modes that comes out to be $\pm e/2$ [57].

As a side mark, we mention here that the topological nature of the phase can also be determined based on the availability of the zero eigenvalues of the local in-gap Green's function as studied in Ref. [58].

2. Bulk-boundary correspondence

As mentioned, the bulk-boundary correspondence refers to the connection between edge and surface states of a finite system to the difference in bulk topological invariants across the QPT [46,59–62]. The topological behavior is associated with the existence of edge states on the boundary of open systems [46], which in turn is complemented by a nonzero Berry phase within the bulk (and vice versa). The edge modes peak at the boundary and decay exponentially towards the bulk. Generally, bulk-boundary correspondence is present in most of the Hermitian systems. However, a more generalized understanding of the same is required for more complicated Hermitian and some non-Hermitian systems [63–65].

For a system with chiral symmetry, one can find a chiral partner for each of the states. For the topological insulators, bulk-boundary relation refers to a one-to-one correspondence between the number of gapless zero-energy end-modes in a topologically nontrivial system and the topological invariant (winding number). For instance, the number of conducting edge states in a 2D quantum Hall system is the same as the Chern number that appears in the transverse conductivity [56]. Unlike in the case of $\theta = \pi$, where end states are restricted in single sublattices, here for $\theta = \pi/2$ the end states are restricted in two sublattices such that no two consecutive sites see nonzero amplitude of them. In other words, the amplitude of the end-state wave functions vanishes in alternate sites (corresponding to two sublattices) while the rest of the sites (corresponding to the other two sublattices) alternately see positive and negative amplitudes, also indicating a gradual decay of strength from the end of the chain towards the bulk. The winding number is equivalent to the net number of end states: $N_A - N_D$, where N_A and N_D are the number of end states of sublattices A and D (that include the two end sites), respectively, on sublattice A on the left end (see pp. 16 and 17 of Ref. [46]). The winding number is estimated from the bulk Hamiltonian while the net number of end states can be obtained by looking at the low-energy sector of the left end. For the trivial case, $\Delta^2/t^2 > 2$, both are 0 and for the topological case, $0 < \Delta^2/t^2 < 2$, both are 1. This indicates that there is one end mode localized in sublattice A and no end mode localized in sublattice D, observed from the left. The corresponding wave functions are shown to be highly located near the ends. Since each chiral pair is connected with opposite energies $\pm\epsilon(k)$, the single end mode must obey it as well, resulting in $\epsilon(k) = 0$. Interestingly, the wave functions of the zero-energy end modes can be explicitly derived without solving the eigenvalue problems and further studied as in Ref. [66].

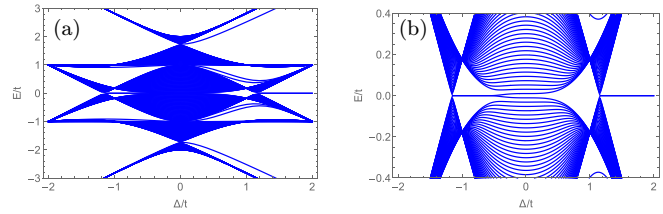

FIG. 4. Spectra of a SSH(-like) chain (considering OBCs) as a function of Δ/t for $\theta = \frac{\pi}{3}$. (b) represents the same zoomed in at low energies. Both plots are for $L = 300$.

Edge states in BDI class are time-reversal symmetric and there can be a phase factor of ± 1. Thus, one may require the correct linear combination of degenerate edge states to notice this symmetry [45].

In the following, we will discuss the cases for two other commensurate θ values. To make the paper precise, we only mention the distinctive features of same.

B. For $\theta = \pi/3$

The chiral symmetry of an odd-n SSH(like) model Eq. (1) is obscured in momentum space, as found in Ref. [53]. Hence, the winding number is also not well-defined for $\theta = 2\pi/3$. Consequently, the chiral symmetry for this case does not give directly to the nontrivial band topology via the winding number. The possible way to make the chiral symmetry more diaphanous is by assembling two neighboring unit cells of the SSH(-like) model (for $\theta = 2\pi/3$) simultaneously to constitute a six-band SSH model as documented in Refs. [53,65]. This six-band SSH model corresponds to $n = 6$ or $\theta = \pi/3$. The corresponding Bloch Hamiltonian will be given by 6×6 matrix H_k as shown in Eq. (C1) of Appendix C.

The numerical spectra for this case is presented in Fig. 4. We see from the plot that energy spectra is symmetric, i.e., for every eigenstate with energy E, its chiral symmetric partner having energy $-E$ necessarily exists. Here, similar to $\theta = \pi/2$, we get a six-sublattice configuration and new gaps can be found within the spectrum. Interestingly we get six in-gap states in TTP while two in-gap states and two midgap ZESs in NTP. Here, similar to $\theta = \pi/2$, ZES no longer exists for all values of $|\Delta/t|$, including $|\Delta/t| = 0$, as shown in Fig. 4(b). The energy gap closes (and reopens) at $|\Delta/t| = 0,\ 2/\sqrt{3}$, indicating three topological QPT points.

The above Hamiltonian has chiral symmetry and also respects time-reversal and particle-hole symmetry. Thus, it belongs to the BDI class in the tenfold-way classification (see Table I). The chiral symmetry exhibits itself as $\Gamma H_k \Gamma = -H_k$ with $\Gamma_{ij} = (-1)^i \delta_{ij}$. The Hamiltonian H_k in Eq. (C1) can be cast into block off-diagonal form as

$$H_k = \begin{pmatrix} 0 & V \\ V^\dagger & 0 \end{pmatrix}, \tag{17}$$

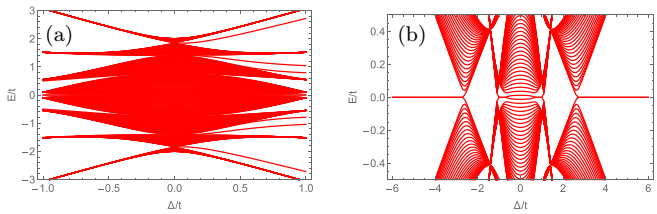

FIG. 5. (a) Spectra of a SSH(-like) chain with OBC as a function of Δ/t with $L = 256$ for $\theta = \frac{\pi}{4}$. (b) represents the same zoomed in at low energies.

with

$$V = \begin{pmatrix} (t+\Delta) & 0 & \left(t+\frac{\Delta}{2}\right)e^{-6ik} \\ \left(t+\frac{\Delta}{2}\right) & \left(t-\frac{\Delta}{2}\right) & 0 \\ 0 & (t-\Delta) & \left(t-\frac{\Delta}{2}\right) \end{pmatrix}. \tag{18}$$

Using a similar approach as shown for the $\theta = \pi/2$ case, one can obtain the winding number for the winding vector **Det**[**V**(**k**)] to be

$$\mathcal{W} = \begin{cases} 1, & 0 > \frac{\Delta}{t} > -2/\sqrt{3} \text{ or } \frac{\Delta}{t} > 2/\sqrt{3} \\ 0, & 0 < \frac{\Delta}{t} < 2/\sqrt{3} \text{ or } \frac{\Delta}{t} < -2/\sqrt{3}. \end{cases} \tag{19}$$

Now, in the parametric plot, similar to the case with $\theta = \pi/2$, the circular contour of winding vector **Det**[**V**(**k**)] for $t^3 - 3t\Delta^2/4 + \Delta^3/4 > (<)\, t^3 - 3t\Delta^2/4 - \Delta^3/4$ would not (would) encircle the origin, suggesting a TTP (NTP) with winding number $\mathcal{W} = 0$ (1). And the contour should pass through the origin for $|\Delta/t| = 0,\ 2/\sqrt{3}$ indicating a gap-closing phase-transition point.

C. For $\theta = \pi/4$

Now we consider a finite chain with $\theta = \frac{\pi}{4}$ for which one obtains an 8×8 Bloch Hamiltonian H_k [see Eq. (C2) of Appendix C]. The numerical spectra for this case is presented in Fig. 5. We see from the plot that the energy spectra is symmetric, i.e., for every eigenstate with energy E, its chiral symmetric partner having energy $-E$ necessarily exists. The spectra confirm eight in-gap states. Out of eight in-gap states, six are found at nonzero energies while two are ZESs. The existence of ZESs with variation of Δ/t is shown in Fig. 5(b). The spectrum shows the gap-closing transitions occur at $|\Delta/t| = \sqrt{2(2 \pm \sqrt{2})}$, which are indeed the four topological QPT points in this case.

Just like in the previous cases, an unitary transformation from there leads to the block diagonalization:

$$H_k \to U H_k U^{-1} = \begin{pmatrix} 0 & V \\ V^\dagger & 0 \end{pmatrix}, \tag{20}$$

with

$$V = \begin{pmatrix} (t+\Delta) & 0 & 0 & \left(t+\frac{\Delta}{\sqrt{2}}\right)e^{-8ik} \\ \left(t+\frac{\Delta}{\sqrt{2}}\right) & t & 0 & 0 \\ 0 & \left(t-\frac{\Delta}{\sqrt{2}}\right) & (t-\Delta) & 0 \\ 0 & 0 & \left(t-\frac{\Delta}{\sqrt{2}}\right) & t \end{pmatrix}. \tag{21}$$

This now helps in estimating the winding number and we obtain

$$\mathcal{W} = \begin{cases} 1, & 0 < \frac{\Delta^2}{t^2} < 2(2-\sqrt{2}) \text{ or } \frac{\Delta^2}{t^2} > 2(2+\sqrt{2}) \\ 0, & 2(2-\sqrt{2}) < \Delta^2/t^2 < 2(2+\sqrt{2}) \\ \text{undefined}, & \Delta^2/t^2 = 2(2 \pm \sqrt{2}). \end{cases} \tag{22}$$

One can again look at the parametric plot of **Det[V(k)]** in the complex plane for all Brillouin zone vectors and find the circular contour to enclose the origin for $\Delta^2/t^2 > (<)\ [2(2 + (-)\sqrt{2})]$, signaling a NTP with winding number $\mathcal{W} = 1$.

For the sake of completeness, we should mention here that a winding number of $\mathcal{W} = -1$ can be obtained in an extended SSH model incorporating longer range hopping between different sublattices [66]. Interestingly, considering more than one further neighbor hopping term, Pérez-González *et al.* (2018) demonstrated how an additional topological phase with $\mathcal{W} = 2$ can be obtained [67]. It shows two individual pairs of topological edge states. Moreover, the topological phases with larger winding numbers (say, up to $\mathcal{W} = 4$) are also found to appear with the inclusion of multiple further neighbor hopping terms [68].

D. End states for different θ's

Features of the end states for different θ were mentioned to some extent in Ref. [12]. Here we give some further details of same for $\theta = \pi$, $\pi/2$, $\pi/3$, and $\pi/4$. Deep within the topological phase, the pair of chiral zero energy end states are obtained for $\theta = \pi$ that survive in single boundaries. However, close to QPT, the end states in NTP survive at both boundaries and in the sublattices containing the end sites. The wave functions oscillate to gradually vanish within the bulk. They are of mixed chirality, which can be combined linearly to yield chiral end modes surviving at single ends of the chain [28]. Similar trends are observed for other θ values as well. For $\theta = 2\pi/n$ with $n > 2$, new in-gap states appear ($n - 2$ in number, i.e., 0, 2 and 6 for n =2, 4, and 8, respectively) in the NTP. They can be called end states as they peak near the chain boundary (not necessarily at end sites though). However, we find only two in-gap states for $n = 6$ in the NTP. Interestingly, there are a few states near the edge of these gaps in the spectrum which show localized peaks near boundaries [see right panel plots of Fig. 6(f)].

III. SSH(-LIKE) CHAIN WITH DOMAIN WALL

To embark on our exploration, we also introduce single domain wall [37] in our SSH(-like) chain with the hopping modulation now taking the form of

$$\delta_i = d_0 \tanh\left[\frac{i - i_0}{\xi/a}\right] \cos[(i-1)\theta], \tag{23}$$

where d_0, ξ, and a are the amplitude of the DW, the width of the DW, and the lattice spacing respectively. Here, i_0 is a parameter that actually determines the position of the DW (in the present study, we consider the location of the DW at the center of the chain). This DW separates the two dimerized phases and the Hamiltonian (we call it $H_{\text{SSH}}^{\text{DW}}$) exhibits fractionalized zero modes at the location of the domain wall [37]. We

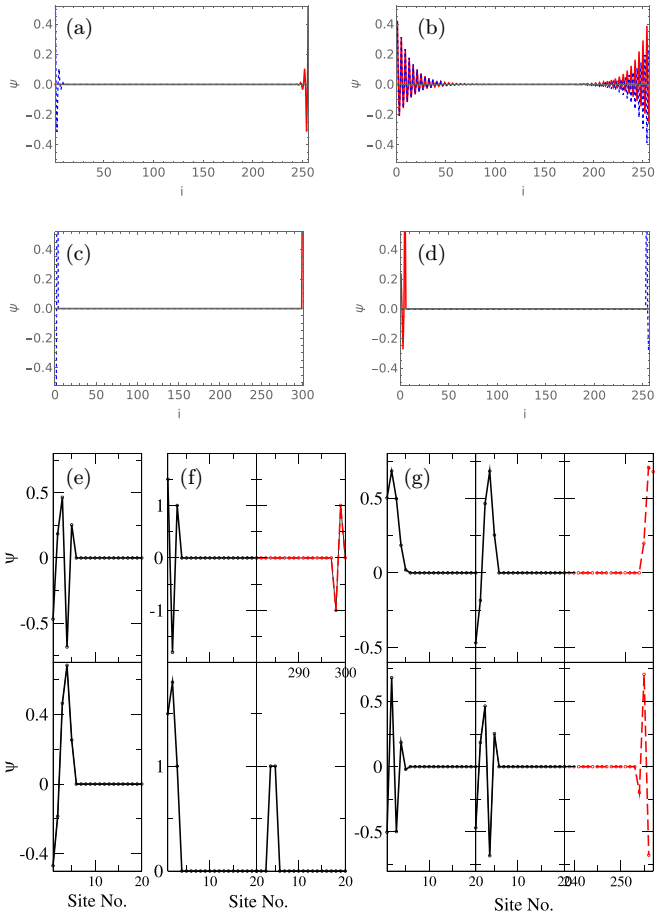

FIG. 6. The midgap ZES of a finite SSH(like) chain for $\theta =$ (a) π, (b) $\pi/2$, (c) $\pi/3$, and (d) $\pi/4$. There are also in-gap end states at nonzero energies, as can be seen for $\theta =$ (e) $\pi/2$, (f) $\pi/3$, and (g) $\pi/4$.

can add here that the boundaries of the SSH(-like) chain we studied so far may be seen as domain walls with the vacuum or surrounding.

In this paper, we probe such systems with a single static domain wall for different values of θ. For instance, the energy spectra of a SSH(-like) chain in the presence of a domain wall as a function of domain wall amplitude d_0 for $\theta = \pi$ and different values of ξ is presented in Fig. 7. We find the DW results in additional in-gap states (often called bound states [37]) other than the midgap ZES, and the gap reduces with an increase of ξ/a. Interestingly, the zero modes disappear for smaller and higher values of amplitude (d_0). One gets a NN tight-binding model at $d_0 = 0$, where no zero energy state is there in a finite system. For small d_0, on the other hand, the availability of topologically protected zero modes depends on the length of the chain. For a longer chain, one gets a smaller d_0 cutoff that denies the existence of the zero mode. The ZES vanishes for very large d_0 as well. In fact, the decay of the end states away from the edges goes as $\sim|\frac{t-d_0}{t+d_0}|$ [12], which indicates a slow decay for both small and large d_0 values. These lead to hybridization of the two degenerate end modes producing symmetric and antisymmetric linear combinations that lie (slightly) above and below the zero energy. The presence of a pair $(E, -E)$ in the energy spectra

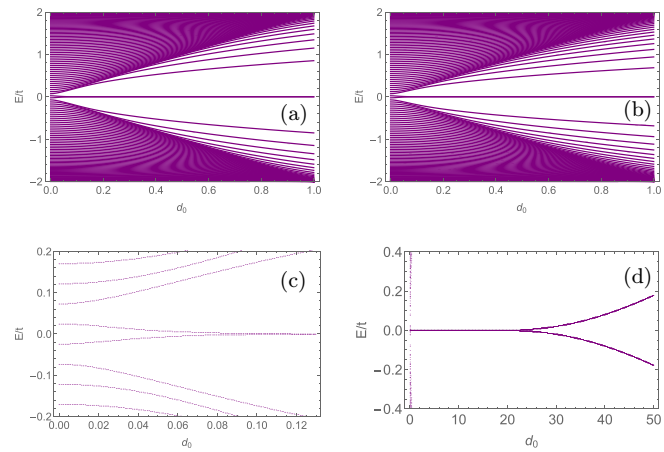

FIG. 7. Upper panels show the energy spectra of a SSH(-like) chain with domain wall for $L = 128$ as a function of domain wall amplitude d_0 with $\theta = \pi$ for (a) $\xi/a = 10$ and (b) $\xi/a = 20$. The bottom panels depict the low-energy spectra for (c) smaller and (d) higher variations of d_0 with $L = 128$ and $\xi/a = 20$.

(see Figs. 7 and 8) ensures the persistence of chirality even after the introduction of the DW [38]. The wave function for zero modes for this case is shown in Fig. 9(a). The figure illustrates that one, among two zero modes, is localized at the DW position and the other at one end of the chain (on the different sublattice than where the domain wall resides). This result implies that the domain walls, similar to the boundary of the SSH chain, host zero-energy localized states. However, the scenario changes for other values of θ.

For $\theta = \pi/2$, there also appear additional in-gap states including topological zero modes, presented in Fig. 8. Like in $\theta = \pi$, ZESs will no longer be present for small and very large values of d_0. More interestingly, for intermediate d_0 values, we

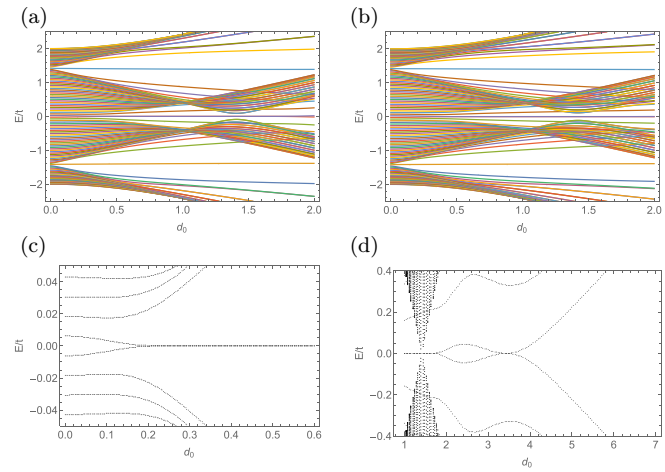

FIG. 8. Top panels present the energy spectra of a SSH(-like) chain with domain wall for $L = 128$ as a function of domain wall amplitude d_0 for $\theta = \pi/2$ with (a) $\xi/a = 10$ and (b) $\xi/a = 16$, respectively. The bottom panels show the corresponding low energy states for (c) smaller and (d) higher d_0 for a chain with $L = 512$ and $\xi/a = 10$.

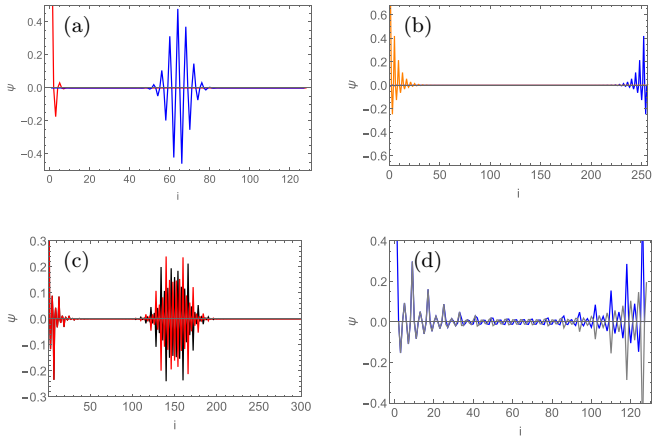

FIG. 9. Zero energy states of SSH(-like) chain in presence of domain wall and for choice of parameters (a) $\theta = \pi$, $d_0 = 0.7$, $\xi/a = 16$, $L = 128$ (b) $\theta = \pi/2$, $d_0 = 0.7$, $\xi/a = 16$, $L = 256$, (c) $\theta = \pi/3$, $d_0 = 0.9$, $\xi/a = 16$, $L = 300$, and (d) $\theta = \pi/4$, $d_0 = 0.9$, $\xi/a = 16$, $L = 128$.

find the zero modes to reappear within a small window of d_0 values [see Fig. 8(d)].

In Fig. 9, we show typical ZESs for $\theta = \pi, \pi/2, \pi/3, \pi/4$. We find the localized states to appear at the DW position only for $\theta = \pi$, $\pi/3$ values, whereas for $\theta = \pi/2$, $\pi/4$ they appear only at the boundaries. In general, these solitonic states appear for $\theta = \frac{\pi}{2p+1}$ with p taking all integer values and they carry a fractional charge of $\pm e/2$ when electrons are spinless [28,57]. The $\pm e/2$ charged state appears when a typical ZES is empty or occupied. In the strong coupling limit ($|\Delta| = t$), there will be an unpaired state on the DW at zero energy. They persist with the reduction of Δ but perish at $\Delta \to 0$. Such typical ZESs are sometimes known as domain wall solitons (kink) and are the physical realization of ZESs found in a one-dimensional field theory proposed by Jackiw and Rebbi (JR) [69].

The SSH model portrays free fermions on a lattice with the hopping strengths alternating between weak and strong bonds and the continuum limit of this model delineates a massive Dirac fermion [70]. On the other hand, the JR model [69] can be viewed as a one-dimensional system where Dirac fermions can be coupled to a soliton field. One can introduce a topological defect (domain wall) familiar as a soliton in the former by changing the arrangements of the hopping strengths (e.g., weak-strong to strong-weak) at a certain lattice site while in the latter by tuning the mass of the fermion such that it changes signs at a certain point. These solitons mark an interface between a nontopological and a topological phase and, accordingly, they have several notable features. For instance, they host localized ZESs, which are characteristic of a transition from nontopological to topological phases and vice versa, and they also hold fractional charges [71]. In the continuum limit, these soliton-induced charge fractionalizations can be ascribed to the local charge operators showing fractional eigenvalues rather than just having fractional expectation values [72]. The ZESs can be called excitations on top of this fractionally charged background and they can be related to MZMs [73].

This soliton appears due to the presence of a single DW. However, the introduction of another DW may lead to the existence of an antisoliton resulting in a soliton and antisoliton pair in the chain. Interestingly, in contrast to polyacetylene, a single DW in graphene nanoribbons can support both a soliton and antisoliton (for more details, see Ref. [28]).

Fascinatingly, the engagement of the DW can also show sharp peaks at the DW position for the in-gap and bound states.

IV. DISORDER

Nowadays, it has become very important to investigate the effect of disorder in electronic systems. Several recent studies have included the behavior of topological systems considering random-dimer disorder [74,75], quasiperiodic disorder [76], and strong disorder [37,77].

This section aims to study numerically the effect of on-site disorder (diagonal) and hopping disorder (of diagonal) on the chirality and zero energy states of the SSH(-like) chain. We introduce on-site disorder via

$$H_{\text{on}}^{\text{disorder}} = \sum_{i=1}^{L} \epsilon_i c_i^{\dagger} c_i, \tag{24}$$

where ϵ_i can be a constant, random (taken from a uniform distribution on $[-G, G]$ [37,77]), staggered (respecting the original two sublattice structure of SSH chain), or interpolated potential. In Ref. [67], the authors considered the on-site energies as the random numbers taken from a Gaussian distribution centered at zero. However, the on-site disorder considered herein is exceedingly similar to the strong disorder mentioned in Refs. [37,77]. We find that the nontriviality of the spectrum and states obtained due to the effect of disorder on the SSH(-like) chain with a multisublattice structure is worth mentioning and is distinct from the pioneer studies [74–77]. The inclusion of the random potential disrupts the chiral symmetry, resulting in the disappearance of fractionalization modes observed at the clean limit (i.e., $G = 0$ or $\epsilon_i = 0$) [37]. Interestingly, however, the end states can retain their chiral nature even for strong (random) on-site disorder due to the effect of Anderson localization [37,78,79].

In this regard, it is worth mentioning RM DW or that of AI class which consider staggered or interpolated on-site potentials as disorder, respectively [38,80]. While SSH and AI domain walls support chiral symmetr- protected ZESs, the RM configuration features DW states at nonzero energies [38,80]. This section is thus devoted to investigating how the chirality-preserving bound states of SSH(-like) chain evolve with disorder of different kinds (i.e., constant, random, staggered, or interpolated ϵ_i) in the presence of the periodic hopping modulations. How the zero modes dissipate their chirality with an increasing disorder strength (G/t or ϵ_i/t) can be understood from the spectrum of the Hamiltonian $H = H_{\text{SSH}}^{\text{DW}} + H_{\text{on}}^{\text{disorder}}$ and is reported in Figs. 10 and 11. The contravention of chiral symmetry affects the energy spectrum which is no longer symmetric, i.e., for every eigenstate having energy E, its chiral symmetric partner with energy $-E$ does not necessarily exist.

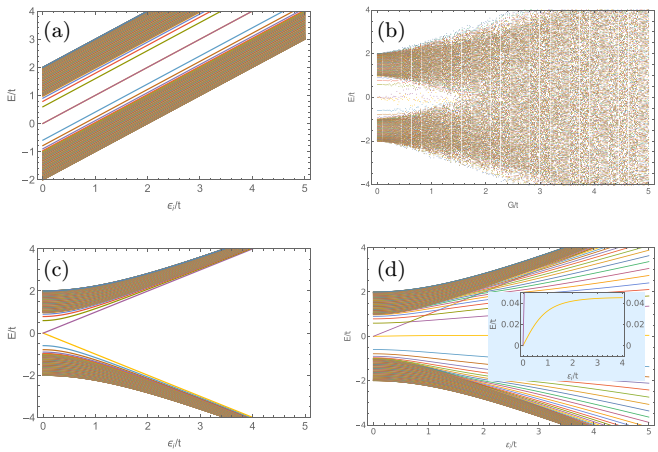

FIG. 10. The energy spectrum of a SSH(-like) chain in presence of various on-site disorders [(a) constant, (b) random, (c) RM type, (d) AI type] for $\theta = \pi$ and a single DW at the center as a function of disorder strength ϵ_i/t or G/t. Other choices of parameters are $L = 256, \xi/a = 10, d_0 = 0.5$. The inset in (d) shows the low energy states.

We find for $\theta = \pi$ and for $L = 256$ and $\xi/a = 10$, the spectrum is legibly divided into two bands with disorder strength (see Fig. 10). The band separation increases (decreases) with ϵ_i/t for RM- and AI-type (random) disorder and the ZES vanishes for nonzero disorder strength. However, for AI-type disorder, a DW state is observed close to zero energy while a random disorder features fluctuating zero modes [37]. Apart from ZESs, several other in-gap states also appear between the two bulk bands for different choices of parameters (such as d_0, ξ/a, and L). In particular, increases in DW amplitude and ξ/a, in turn, give rise to an increase in the number of in-gap states. An infinite SSH chain can have unpaired zero-energy states but a finite chain with open boundaries always leads to paired zero-energy states [81]. We can mention here a related model called Shiozaki-Sato-Gomi model that features constant NN hopping but staggered on-site potentials and obeys a nonsymmorphic chiral symmetry. In contrast to the SSH model, this model supports unpaired zero-energy states at the position of a smooth DW and not at sharp interfaces with vacuum (see Ref. [81]).

For $\theta = \pi/2$, $\theta = \pi/3$, or $\pi/4$, we find that the periodically hopping modulated SSH model with AI DW disorder retrieves the ZES with an increase in disorder strength ϵ_i/t (see Fig. 11). These ZESs are located at the position of the DW. For random-type disorder, the energy gap closes with the increase of G/t. The number of in-gap states as well as the critical disorder strength of the closure of the energy gap decreases as θ is reduced in the commensurate manner as considered in this paper. Considering the commensurate θ values and taking into account the various on-site disorders, one can see that there is no such remarkable change in the energy spectrum.

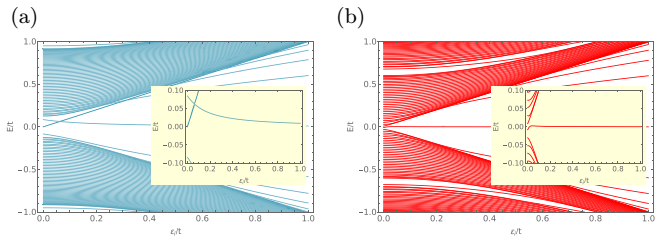

FIG. 11. The ordered energy eigenvalues of a SSH(-like) chain in the presence of an AI-type DW/disorder for (a) $\theta = \pi/2$ and (b) $\theta = \pi/4$ as a function of disorder strength ϵ_i/t with the same choice of parameter as in Fig. 10. The insets show the low energy states.

Other than the on-site potential, disorder can come as hopping parameters as well. The study of the chiral-symmetry-preserving hopping disorder via the Hamiltonian

$$H_{\text{hop}}^{\text{disorder}} = \sum_{i=1}^{L-1} \tau_i (c_{i+1}^{\dagger} c_i + c_i^{\dagger} c_{i+1}), \tag{25}$$

with τ_i randomly generated from a uniform distribution, have shown polarization, as a real space estimator of topological invariance, to continuously reduce to zero with increasing disorder strength for both edge and domain wall states, though their localization remains intact for all disorder strengths [37]. Unlike the on-site disorder, the hopping disorder respects the chiral symmetry. Consequently, the robustness of the DW and edge states are expected in the presence of this kind of disorder. However, notice that the Hamiltonian $H_{\text{hop}}^{\text{disorder}}$ merely renormalizes the hopping parameters of $H_{\text{SSH}}^{\text{DW}}$. This type of perturbation preserves sublattice symmetry which, in turn, gives nonfluctuating zero-energy modes. A strong hopping disorder, however, destroys their chirality, resulting in fluctuating zero energy modes [37,77]. Here, we mention the related AIII chiral-symmetric system which breaks its chiral symmetry at critical disorder strength, resulting in abrupt changes in winding number from 1 to 0 [77]. Moreover, this abrupt change in winding number in the presence of strong hopping disorder for the SSH chain with periodic modulated hopping is worth studying and we will leave this issue for future communication.

V. SUMMARY

In this paper, we have tried to accumulate important findings on the SSH model spectra and topology as well as the midgap zero energy states in the absence as well as presence of DW and disorder and, at the same time, adding insights into same while introducing additional periodic modulation in the hopping parameter. First, without artificial domain walls and disorder, we find that for hopping modulation with commensurate frequency, new in-gap end-states appear—more for smaller values of it. The topological regime shows an interesting variation with θ. We find one, two, three, and four topological phase transition points for $\theta = \pi$, $\pi/2$, $\pi/3$, and $\pi/4$, respectively. In the presence of a static DW that has been put artificially at the center of a finite chain, one end state gets depleted while one ZES appears at the position of the DW for $\theta = \frac{\pi}{2p+1}$ for zero or an integer p value. Unlike the SSH-type DW, an AI-type DW for the model doesn't support chiral symmetry-protected ZESs while an RM DW shows both the edge and domain wall states to be at nonzero energies. However, an on-site disorder always disrupts the system's chirality. With the commensurate reduction of θ, more

in-gap states appear and the ZES of a clean system moves to nonzero energies, though for AI-type disorder, the DW state reaches close to zero energy with disorder strength. A hopping disorder, on the other hand, doesn't contribute much new physics in this regard, as a weak hopping disorder still respects the chiral symmetry.

One can verify these results of hopping-modulated SSH(-like) chains in cold atom systems within optical lattices [82], or maybe in specially designed graphene nanoribbons [83] or topological acoustic systems [84]. Experimental confirmation of similar outcomes can lead to further manipulation of these periodically modulated hopping models to look for more exotic behavior. Down the line, we also have plans to study the-out of-equilibrium behavior of such an extended SSH model, subjected to a quantum quench which has shown to lead to an effective metal insulator transition for $\theta = \pi$ [85]. For a high-frequency periodic quench, it would also be interesting to do a Floquet analysis [86] and probe the competition between the topology and the time periodic driving in our SSH(-like) models.

ACKNOWLEDGMENTS

S.K. thanks G. Baskaran, H. Yao, B. Kumar, S. Basu, S. Mandal, and A. Saha for fruitful discussions. This work is financially supported by DST-SERB, Government of India via Grant No. CRG/2022/002781.

APPENDIX A: WINDING NUMBER IN TERMS OF POLES AND ZEROS

The winding number can be defined in terms of poles and zeros of $\mathbf{Det}[\mathbf{V}(\mathbf{k})] = f(k)$ as a function of a complex variable $z(k) = e^{-ik}$ inside the unit circle. Accordingly, the winding number becomes [87]

$$\mathcal{W} = \frac{1}{2\pi i}\oint_{|z|=1}\frac{f'(z)}{f(z)}dz. \tag{A1}$$

Here, in the complex plane, the closed curve represents the anticlockwise path around the unit circle. Considering the number of zeros (U_f) and number of poles (V_f) of $f(z)$ enclosed by the curve, one can write, following Cauchy's argument principle of complex analysis [47,88],

$$\mathcal{W} = U_f - V_f. \tag{A2}$$

Every zero and pole are weighted by their multiplicity [89] and order, respectively. It is presumed that there are no zeros and poles on the curve. So, for this present case of $\theta = \pi/2$, we get $f(z) = (t^2 - \Delta^2) + t^2 z$. $f(z)$ contains no poles, but it has a zero of multiplicity one:

$$f[-(t^2 - \Delta^2)/t^2] = f(z_0) = 0.$$

The zero is inside the unit circle if $|t^2 - \Delta^2| < |t^2|$. Therefore, Eq. (A2) gives

$$\mathcal{W} = U_f - V_f = \begin{cases} 1 - 0 = 1, & 0 < \Delta^2/t^2 < 2 \\ 0, & \Delta^2/t^2 > 2 \\ \text{undefined}, & \Delta/t = 0, \end{cases} \tag{A3}$$

which is the same as Eq. (14). If $\Delta/t = 0$, then the spectrum is considered to be conducting and the representation of topological invariants is not well-defined. For this case, contrary to the above conjecture, the zero of $f(z)$ arises at $z_0 = -1$, which is on the unit circle.

APPENDIX B: BERRY PHASE

Another topological invariant of this 1D system is the Zak phase. The bulk-boundary correspondence affirms that the presence of edge states is related to the nonzero topological invariant of the bulk. In particular, the number of edge modes on every edge is exactly equal to $|\mathcal{W}|$. The Zak phase γ [90–92] of the system corresponds to $\pi\mathcal{W}$ (eventually, depending on the convention, modulo 2π). Closing of the energy gap (for $\Delta/t = 0$, in this case), and a subsequent reopening at the Brillouin zone boundaries indicates that the system may go through a topological phase transition. In addition, the appearance of a nonzero topological invariant in one of the gapped phases ensures the advent of nontrivial topology. This topological invariant is expressed in terms of the Zak phase, which is purely a bulk property of the system. Therefore, we need to make sure of the accomplishment of the Born-von Karman periodic boundary condition.

It is known that the 1D winding number in the SSH model is closely related to the Zak phase [92], which is basically similar to the Berry phase (γ) [93] for 1D systems. Consequently, it is related to the winding number as $\gamma = \pi\mathcal{W}$. So, the Berry phase becomes

$$\gamma = \begin{cases} \pi, & 0 < \Delta^2/t^2 < 2 \\ 0, & \Delta^2/t^2 > 2 \\ \text{undefined}, & \Delta/t = 0. \end{cases} \tag{B1}$$

APPENDIX C: BLOCH HAMILTONIAN MATRIX FOR $\theta = \frac{\pi}{3}$ AND $\theta = \frac{\pi}{4}$

The Bloch Hamiltonian in the case of $\theta = \pi/3$ is given in Eq. (C1), in which $z = e^{-6ik}$. Here, the unit cell contains six sublattices, so the size of the BZ boundary further reduces, i.e., $k \in [-\pi/6,\ \pi/6]$:

$$H_k = \begin{pmatrix} 0 & (t+\Delta) & 0 & 0 & 0 & \left(t+\frac{\Delta}{2}\right)z \\ (t+\Delta) & 0 & \left(t+\frac{\Delta}{2}\right) & 0 & 0 & 0 \\ 0 & \left(t+\frac{\Delta}{2}\right) & 0 & \left(t-\frac{\Delta}{2}\right) & 0 & 0 \\ 0 & 0 & \left(t-\frac{\Delta}{2}\right) & 0 & (t-\Delta) & 0 \\ 0 & 0 & 0 & (t-\Delta) & 0 & \left(t-\frac{\Delta}{2}\right) \\ \left(t+\frac{\Delta}{2}\right)z^* & 0 & 0 & 0 & \left(t-\frac{\Delta}{2}\right) & 0 \end{pmatrix}. \tag{C1}$$

The Bloch Hamiltonian for $\theta = \pi/4$ is calculated as in Eq. (C2). Here, eight sublattices are embedded in a unit cell which can further partition the BZ boundary. Thus, in the reduced BZ, $k \in [-\pi/8,\ \pi/8]$:

$$H_k = \begin{pmatrix} 0 & (t+\Delta) & 0 & 0 & 0 & 0 & 0 & \left(t+\frac{\Delta}{\sqrt{2}}\right)e^{-8ik} \\ (t+\Delta) & 0 & \left(t+\frac{\Delta}{\sqrt{2}}\right) & 0 & 0 & 0 & 0 & 0 \\ 0 & \left(t+\frac{\Delta}{\sqrt{2}}\right) & 0 & t & 0 & 0 & 0 & 0 \\ 0 & 0 & t & 0 & \left(t-\frac{\Delta}{\sqrt{2}}\right) & 0 & 0 & 0 \\ 0 & 0 & 0 & \left(t-\frac{\Delta}{\sqrt{2}}\right) & 0 & (t-\Delta) & 0 & 0 \\ 0 & 0 & 0 & 0 & (t-\Delta) & 0 & \left(t-\frac{\Delta}{\sqrt{2}}\right) & 0 \\ 0 & 0 & 0 & 0 & 0 & \left(t-\frac{\Delta}{\sqrt{2}}\right) & 0 & t \\ \left(t+\frac{\Delta}{\sqrt{2}}\right)e^{8ik} & 0 & 0 & 0 & 0 & 0 & t & 0 \end{pmatrix}. \tag{C2}$$

[1] C. Nayak, S. H. Simon, A. Stern, M. Freedman, and S. Das Sarma, Non-Abelian anyons and topological quantum computation, Rev. Mod. Phys. **80**, 1083 (2008).

[2] S. R. Elliott and M. Franz, Colloquium: Majorana fermions in nuclear, particle, and solid-state physics, Rev. Mod. Phys. **87**, 137 (2015).

[3] C. Beenakker, Search for Majorana fermions in superconductors, Annu. Rev. Condens. Matter Phys. **4**, 113 (2013).

[4] F. Wilczek, Majorana returns, Nat. Phys. **5**, 614 (2009).

[5] H. Ren, F. Pientka, S. Hart, A. T. Pierce, M. Kosowsky, L. Lunczer, R. Schlereth, B. Scharf, E. M. Hankiewicz, L. W. Molenkamp *et al.*, Topological superconductivity in a phase-controlled Josephson junction, Nature (London) **569**, 93 (2019).

[6] V. Mourik, K. Zuo, S. M. Frolov, S. R. Plissard, E. P. A. M. Bakkers, and L. P. Kouwenhoven, Signatures of Majorana fermions in hybrid superconductor-semiconductor nanowire devices, Science **336**, 1003 (2012).

[7] M. Leijnse and K. Flenzberg, Introduction to topological superconductivity and Majorana fermions, Semicond. Sci. Technol. **27**, 124003 (2012).

[8] P. Hosur, P. Ghaemi, R. S. K. Mong, and A Vishwanath, Majorana modes at the ends of superconductor vortices in doped topological insulators, Phys. Rev. Lett. **107**, 097001 (2011).

[9] J. Klinovaja, S. Gangadharaiah, and D. Loss, Electric-field-induced Majorana fermions in armchair carbon nanotubes, Phys. Rev. Lett. **108**, 196804 (2012).

[10] J. D. Sau and S. Das Sarma, Realizing a robust practical Majorana chain in a quantum-dot-superconductor linear array, Nat. Commun. **3**, 964 (2012).

[11] J. Fu, Majorana orthogonal transformation and Majorana zero modes in free fermionic systems, Ann. Phys. **432**, 168564 (2021).

[12] S. Kar, Edge state behavior in a Su–Schrieffer–Heeger like model with periodically modulated hopping, J. Phys.: Condens. Matter **36**, 065301 (2024).

[13] J. Sau and S. Tewari, Chapter Four-Topological superconductivity in spin-orbit-coupled semiconducting nanowires, Semicond. Semimet. **108**, 125 (2021).

[14] R. Pawlak *et al.*, Majorana fermions in magnetic chains, Prog. Part. Nucl. Phys. **107**, 1 (2019).

[15] G. Vidal, Efficient classical simulation of slightly entangled quantum computations, Phys. Rev. Lett. **91**, 147902 (2003).

[16] R. Horodecki, P. Horodechi, M. Horodechi, and K. Horodechi, Quantum entanglement, Rev. Mod. Phys. **81**, 865 (2009).

[17] K. S. Novoselov *et al.*, Electric field effect in atomically thin carbon films, Science **306**, 666 (2004).

[18] S. Das Sarma, S. Adam, E. H. Hwang, and E. Rossi, Electronic transport in two-dimensional graphene, Rev. Mod. Phys. **83**, 407 (2011).

[19] F. D. M. Haldane, Model for a quantum Hall effect without Landau levels: Condensed-matter realization of the "parity anomaly, Phys. Rev. Lett. **61**, 2015 (1988).

[20] C. L. Kane and E. J. Mele, Quantum spin Hall effect in graphene, Phys. Rev. Lett. **95**, 226801 (2005).

[21] M. Z. Hasan, and C. L. Kane, Colloquium: Topological insulators, Rev. Mod. Phys. **82**, 3045 (2010).

[22] S. Kar, A. Jayannavar, A primer on Weyl semimetals: Down the discovery of topological phases, Asian J. Res. Rev. Phys. **4**, 34 (2021).

[23] R. Heyrovska, Atomic structures of graphene, benzene and methane with bond lengths as sums of the single, double and resonance bond radii of carbon, arXiv:0804.4086.

[24] L. Salem, *The Molecular Orbital Theory of Conjugated Systems* (W. A. Benjamin, New York, 1966), pp. 516–523.

[25] W. P. Su, J. R. Schrieffer, and A. J. Heeger, Solitons in polyacetylene, Phys. Rev. Lett. **42**, 1698 (1979).

[26] W. P. Su, J. R. Schrieffer, and A. J. Heeger, Soliton excitations in polyacetylene, Phys. Rev. B **22**, 2099 (1980).

[27] A. J. Heeger, S. Kivelson, J. R. Schrieffer, and W.-P. Su, Solitons in conducting polymers, Rev. Mod. Phys. **60**, 781 (1988).

[28] S.-R. Eric Yang, Soliton fractional charges in graphene nanoribbon and polyacetylene: Similarities and differences, Nanomaterials **9**, 885 (2019).

[29] E. J. Meier *et al.*, Observation of the topological soliton state in the Su–Schrieffer–Heeger model, Nat. Commun. **7**, 13986 (2016).

[30] N. T. Ziani, C. Fleckenstein, L. Vigliotti, B. Trauzettel, and M. Sassetti, From fractional solitons to Majorana fermions in a paradigmatic model of topological superconductivity, Phys. Rev. B **101**, 195303 (2020).

[31] A. Y. Kitaev, Unpaired Majorana fermions in quantum wires, Phys. Usp. **44**, 131 (2001).

[32] Reference [12] is overambitious in calling the zero energy modes of SSH(-like) chains Majorana modes. In fact, a pair of Majorana modes of different flavors localized at each end is superposed to yield electronic end modes there.

[33] F. M. D'Angelis, F. A. Pinheiro, D. Guery-Odelin, S. Longhi, and F. Impens, Fast and robust quantum state transfer in a topological Su-Schrieffer-Heeger chain with next-to-nearest-neighbor interactions, Phys. Rev. Res. **2**, 033475 (2020).

[34] F. Munoz, F. Pinilla, J. Mella, and M. I. Molina, Topological properties of a bipartite lattice of domain wall states, Sci. Rep. **8**, 17330 (2018).

[35] S. Longhi, Topological pumping of edge states via adiabatic passage, Phys. Rev. B **99**, 155150 (2019).

[36] L. Qi, Y. Yan, Y. Xing, X. D. Zhao, S. Liu, W. X. Cui, X. Han, S. Zhang, and H. F. Wang, Topological router induced via long-range hopping in a Su-Schrieffer-Heeger chain, Phys. Rev. Res. **3**, 023037 (2021).

[37] M. Scollon and M. P. Kennett, Persistence of chirality in the Su-Schrieffer-Heeger model in the presence of on-site disorder, Phys. Rev. B **101**, 144204 (2020).

[38] S.-H. Han *et al.*, Topological domain-wall states hosting quantized polarization and Majorana zero modes without bulk boundary correspondence, arXiv:2311.08771.

[39] We should note here that the first quantized single particle chiral symmetric Hamiltonian reverses sign under the chiral symmetry operation (see also Sec. II A 1). This sign change is, however, compensated by the anticommutivity of the fermionic operators to produce the invariance of the second quantized Hamiltonian [41,47]. A Fourier transformed second quantized SSH Hamiltonian, written as $H = \sum (a_k^\dagger b_k^\dagger) H_k (a_k b_k)^T$ as in Ref. [12], reserves its sign under the second quantized chiral symmetry transformation given as $a_k(b_k) \to b_k^\dagger(a_k^\dagger)$, $H_k \to -H_k$.

[40] B. A. Bernevig and T. L. X. Hughes, *Topological Insulators and Topological Superconductors* (Princeton University Press, Cambridge, 2013).

[41] A. Ludwig, Topological phases: Classification of topological insulators and superconductors of non-interacting fermions, and beyond, Phys. Scr. **2016**, 014001 (2016).

[42] C.-K. Chiu, J. C. Y. Teo, A. P. Schnyder, and S. Ryu, Classification of topological quantum matter with symmetries, Rev. Mod. Phys. **88**, 035005 (2016).

[43] A. Altland and M. R. Zirnbauer, Novel symmetry classes in mesoscopic normal-superconducting hybrid structures, Phys. Rev. B **55**, 1142 (1997).

[44] Even though the hopping strength is complex, one can consider a gauge transformation $c_j \to e^{i\alpha_j} c_j$ to get the hopping amplitudes real again. In other words, even with complex hopping strength, the model retains time-reversal symmetry by defining the correct time-reversal operator.

[45] P. Matveeva, T. Hewitt, D. Liu, K. Reddy, D. Gutman, and S. T. Carr, One-dimensional noninteracting topological insulators with chiral symmetry, Phys. Rev. B **107**, 075422 (2023).

[46] J. K. Asbóth, L. Oroszlány, and A. Pályi, *A Short Course on Topological Insulators* (Springer International Publishing, AG Switzerland, 2016).

[47] O. Balabanov, D. Erkensten, and H. Johannesson, Topology of critical chiral phases: Multiband insulators and superconductors, Phys. Rev. Res. **3**, 043048 (2021).

[48] V. Gurarie, Single-particle Green's functions and interacting topological insulators, Phys. Rev. B **83**, 085426 (2011).

[49] Z. Wang and S. C. Zhang, Topological invariants and ground-state wave functions of topological insulators on a torus, Phys. Rev. X **4**, 011006 (2014).

[50] S. Bid and A. Chakrabarti, Topological properties of a class of Su-Schrieffer-Heeger variants, Phys. Lett. A **423**, 127816 (2022).

[51] Y. Lin, W. Hao, M. Wang *et al.*, Topological superconductors from one-dimensional periodically modulated Majorana chains, Sci. Rep. **7**, 9210 (2017).

[52] S. Ryu, A. P. Schnyder, A. Furusaki, and A. W. W. Ludwig, Topological insulators and superconductors: Tenfold way and dimensional hierarchy, New J. Phys. **12**, 065010 (2010).

[53] Y. He and C.-C. Chien, Non-Hermitian generalizations of extended Su–Schrieffer–Heeger models, J. Phys.: Condens. Matter **33**, 085501 (2021).

[54] M. McIntyre and G. Cairns, A new formula for winding number, in *Geometriae Dedicata* (1993), Vol. 46, pp. 149–159.

[55] T. O. Puel, P. D. Sacramento, and M. A. Continentino, 4π Josephson currents in junctions of hybridized multiband superconductors, Phys. Rev. B **95**, 094509 (2017).

[56] M. Maffei, A. Dauphin, F. Cardano, M. Lewenstein, and P. Massignan, Topological characterization of chiral models through their long time dynamic, New J. Phys. **20**, 013023 (2018).

[57] C. L. Kane, *Topological Band Theory and the $\mathcal{Z}_2$ Invariant*, Contemporary Concepts of Condensed Matter Science Vol. 6 (Elsevier, Amsterdam, 2013), Chap. 1, pp. 3–34.

[58] R.-J. Slager, L. Rademaker, J. Zaanen, and L. Balents, Impurity-bound states and Green's function zeros as local signatures of topology, Phys. Rev. B **92**, 085126 (2015).

[59] N. Batra and G. Sheet, Physics with Coffee and Doughnuts, Resonance **25**, 765 (2020).

[60] N. Sedlmayr, P. Jaeger, M. Maiti, and J. Sirker, Bulk-boundary correspondence for dynamical phase transitions in one-dimensional topological insulators and superconductors, Phys. Rev. B **97**, 064304 (2018).

[61] R. Koch and J. C. Budich, Bulk-boundary correspondence in non-Hermitian systems: Stability analysis for generalized boundary conditions, Eur. Phys. J. D **74**, 70 (2020).

[62] E. Prodan and H. Schulz-Baldes, *Bulk and Boundary Invariants for Complex Topological Insulators: From K-Theory to Physics* (Springer, Switzerland, 2016).

[63] K. Yokomizo and S. Murakami, Non-Bloch band theory of non-Hermitian systems, Phys. Rev. Lett. **123**, 066404 (2019).

[64] Y. Xiong, Why does bulk boundary correspondence fail in some non-Hermitian topological models, J. Phys. Commun. **2**, 035043 (2018).

[65] A. Anastasiadis, G. Styliaris, R. Chaunsali, G. Theocharis, and F. K. Diakonos, Bulk-edge correspondence in the trimer Su-Schrieffer-Heeger model, Phys. Rev. B **106**, 085109 (2022).

[66] C. Li and A. E. Miroshnichenko, Extended SSH Model: Non-local couplings and non-monotonous edge states, Physics **1**, 2 (2019); S.-L. Zhang, Q. Zhou, Two-leg Su-Schrieffer-Heeger chain with glide reflection symmetry, Phys. Rev. A **95**, 061601(R) (2017).

[67] B. Pérez-González, M. Bello, A. Gómez-Lón, and G. Platero, SSH model with long-range hoppings: Topology, driving and disorder, arXiv:1802.03973.

[68] A. Ghosh, A. M. Martin, and S. Majumder, Quench dynamics of edge states in a finite extended Su-Schrieffer-Heeger system, arXiv:2303.00269.
[69] R. Jackiw and C. Rebbi, Solitons with fermion number 1/2, Phys. Rev. D **13**, 3398 (1976).
[70] R. Jackiw and J. Schrieffer, Solitons with fermion number 1/2 in condensed matter and relativistic field theories, Nucl. Phys. B **190**, 253 (1981).
[71] J. Goldstone and F. Wilczek, Fractional quantum numbers on solitons, Phys. Rev. Lett. **47**, 986 (1981).
[72] R. Jackiw, A. Kerman, I. Klebanov, and G. Semenoff, Fluctuations of fractional charge in soliton anti-soliton systems, Nucl. Phys. B **225**, 233 (1983).
[73] D. X. Horváth, S. Fraenkel, S. Scopa, and C. Rylands, Charge-resolved entanglement in the presence of topological defects, Phys. Rev. B **108**, 165406 (2023).
[74] Z.-S. Xu *et al.*, Observation of reentrant metal-insulator transition in a random-dimer disordered SSH lattice, arXiv:2307.05207.
[75] Z.-W. Zuo and D. Kang, Reentrant localization transition in the Su-Schrieffer-Heeger model with random-dimer disorder, Phys. Rev. A **106**, 013305 (2022).
[76] T. Liu and H. Guo, Topological phase transition in the quasiperiodic disordered Su-Schrieffer-Heeger chain, Phys. Lett. A **382**, 3287 (2018).
[77] I. Mondragon-Shem, T. L. Hughes, J. Song, and E. Prodan, Topological criticality in the chiral-symmetric AIII class at strong disorder, Phys. Rev. Lett. **113**, 046802 (2014).
[78] B. Pérez-González, M. Bello, Á. Gómez-León, and G. Platero, Interplay between long-range hopping and disorder in topological systems, Phys. Rev. B **99**, 035146 (2019).
[79] P. W. Anderson, Absence of diffusion in certain random lattices, Phys. Rev. **109**, 1492 (1958).
[80] S.-H. Han, S. G. Jeong, S. W. Kim, T. H. Kim, and S. Cheon, Topological features of ground states and topological solitons in generalized Su-Schrieffer-Heeger models using generalized time-reversal, particle-hole, and chiral symmetries, Phys. Rev. B **102**, 235411 (2020).
[81] W. Brzezicki and T. Hyart, Topological domain wall states in a nonsymmorphic chiral chain, Phys. Rev. B **101**, 235113 (2020).
[82] D. Xie *et al.*, Topological characterizations of an extended Su–Schrieffer–Heeger model, npj Quantum Inf. **5**, 55 (2019).
[83] O. Gröning *et al.*, Engineering of robust topological quantum phases in graphene nanoribbons, Nature (London) **560**, 209 (2018).
[84] Z. Yang, F. Gao, X. Shi, X. Lin, Z. Gao, Y. Chong, and B. Zhang, Topological acoustics, Phys. Rev. Lett. **114**, 114301 (2015).
[85] S. Porta, N. T. Ziani, D. M. Kennes, F. M. Gambetta, M. Sassetti, and F. Cavaliere, Effective metal-insulator nonequilibrium quantum phase transition in the Su-Schrieffer-Heeger model, Phys. Rev. B **98**, 214306 (2018).
[86] V. Dal Lago, M. Atala, and L. E. F. Foa Torres, Floquet topological transitions in a driven one-dimensional topological insulator, Phys. Rev. A **92**, 023624 (2015).
[87] B.-H. Chen and D.-W. Chiou, An elementary rigorous proof of bulk-boundary correspondence in the generalized Su-Schrieffer-Heeger model, Phys. Lett. A **384**, 126168 (2020).
[88] G. B. Arfken, H. J. Weber, and F. E Harris, *Mathematical Methods for Physicists: A Comprehensive Guide* (Academic Press, New York, 2011).
[89] A zero in the form $a_x(z - z_0)^x$ has a multiplicity x and a pole in the form $a_y = \frac{1}{(z-z_0)^y}$ has an order y.
[90] J. W. Rhim, J. Behrends, and J. H. Bardarson, Bulk-boundary correspondence from the intercellular Zak phase, Phys. Rev. B **95**, 035421 (2017).
[91] C.-S. Lee, I.-F. Io, and H.-C. Kao, Winding number and Zak phase in multi-band SSH models, Chin. J. Phys. **78**, 96 (2022).
[92] J. Zak, Berry's phase for energy bands in solids, Phys. Rev. Lett. **62**, 2747 (1989).
[93] M. V. Berry, Quantal phase factors accompanying adiabatic changes, Proc. R. Soc. London A **392**, 45 (1984).